Supporting information of

How size, shape and assembly of magnetic nanoparticles give rise to different hyperthermia scenarios.

H. Gavilán,[a,b] K. Simeonidis,[*c] E. Myrovali,[d] E. Mazarío,[a,e] O. Chubykalo-Fesenko,[a] R. Chantrell,[f] Ll. Balcells,[g] M. Angelakeris[d], M.P. Morales[*,a] and D. Serantes[*,f]

1. Examples of simulated hysteresis loops

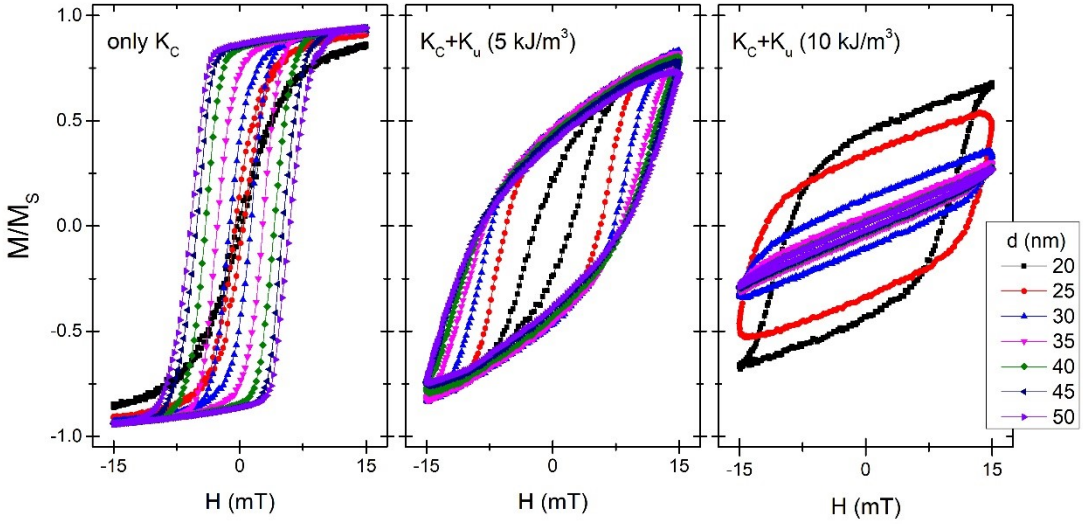

Fig. S1. Representative simulated hysteresis loops of ensemble of non-interacting particle systems of different sizes, with diameters ranging between 20 to 50 nm. The field frequency and amplitude are f = 765 kHz, Hmax = 15 mT, respectively. The left panel corresponds to particles with only cubic magnetocrystalline anisotropy, and centre and right panels correspond to cases with an additional uniaxial term, of value Ku = 5 kJ/m^3 (centre panel) and 10 kJ/m3 (right panel).

The results displayed in Fig. S1 show characteristic distinct features of dynamical properties of systems of magnetic nanoparticles: for a small anisotropy, the increase of the nanoparticle size tends to open the loops (thus producing higher losses). Increasing the anisotropy -in this case by adding a uniaxial term-, results in wider hysteresis loops, therefore releasing more heat but also requiring higher fields to reach saturation. A delicate balance can therefore be established between particle and field amplitude: for small K, increasing the size results in bigger loop areas, but eventually this will lead to minor loops detrimental for heat dissipation.

2. HRTEM analysis of spindles and disks

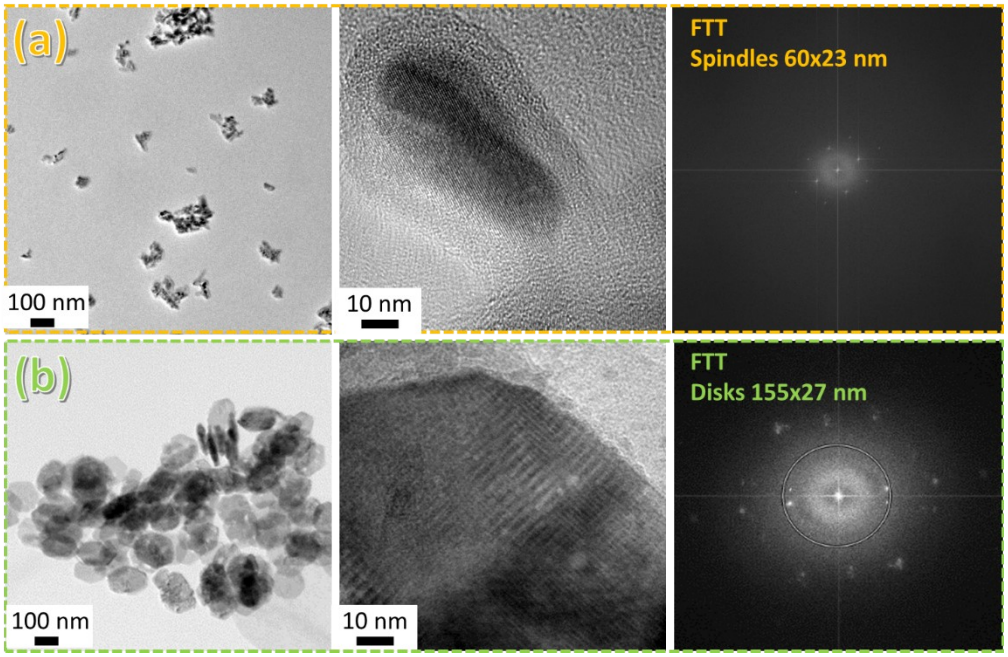

Fig. S2. HRTEM Images of spindles (a) and disks (b) obtained through indirect synthetic routes, showing images at both lower and higher magnification and their corresponding Fourier transform images. Note that the internal porosity is evidenced by dark contrast differences in the images as a consequence of inhomogeneous material density but the FTT diagrams correspond to a monocrystal.

3. DLS Analysis of the MNPs with different morphology and sizes

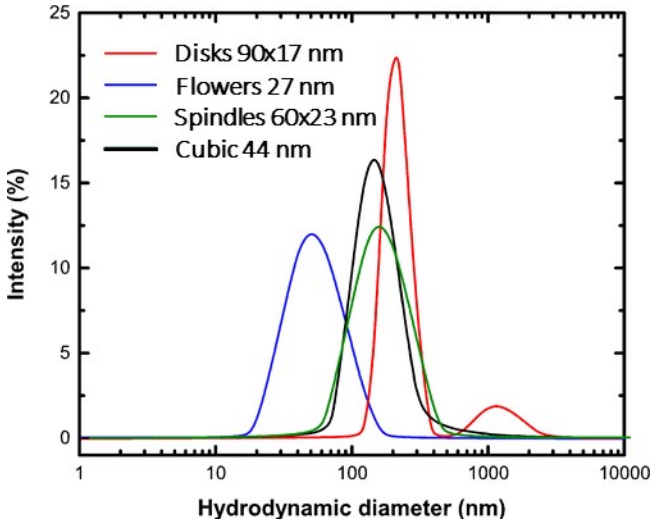

Fig. S3. Hydrodynamic sizes analyzed by DLS in the water dispersions of the following morphology represented in intensity mode: disks 90x17 nm (red line); flowers 27 nm (blue lines); spindles 60x23 nm (light green) and nanocubes 44 nm (dark green).

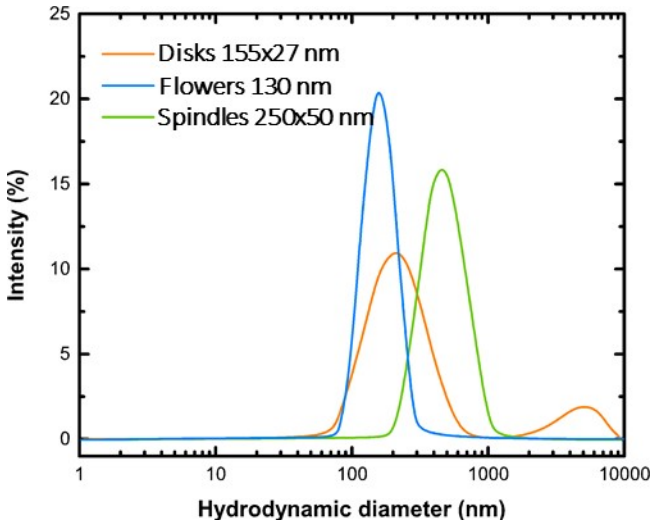

Fig. S4. Hydrodynamic sizes analyzed by DLS in the water dispersions of the following morphologies represented in intensity mode: disks 155x27 nm (yellow line); flowers 130 nm (blue line) and spindles 250x50 nm (light green).

4. DC Hysteresis loops at room temperature of the MNPs with different morphologies and sizes

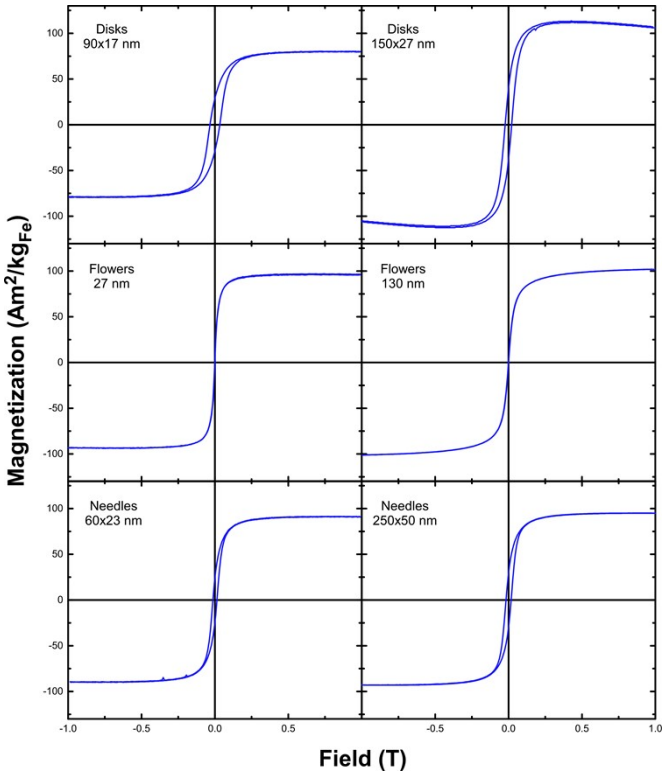

Fig. S5. Room temperature magnetic hysteresis loops studies samples: 90x17 nm disks; 155x27 nm disks; 27 nm flowers; 130 nm flowers; 60x23nm spindles and 250x50 nm spindles.

Table S1. Calculation of magnetic moment per particle for the studied samples.

Sample	Dimensions (nm)	M_s (Am^2/kg_{Fe})	Mass per particle (10^{-16} g)	Moment per particle (10^{-15} Am^2/kg_{Fe})
Disks	90×17	81	5.5	38.7
	155×27	113	16.3	115
Needles	60×23	90	0.85	6.0
	250×50	95	16.7	117
Flowers	27	97	0.53	3.7
	130	103	58.7	412
Cubic	22	113	0.54	3.8
	44	120	4.3	30.5

5. Heating/cooling curves of the samples in different media at frequency 765 kHz and magnetic field intensity of 24 kA/m

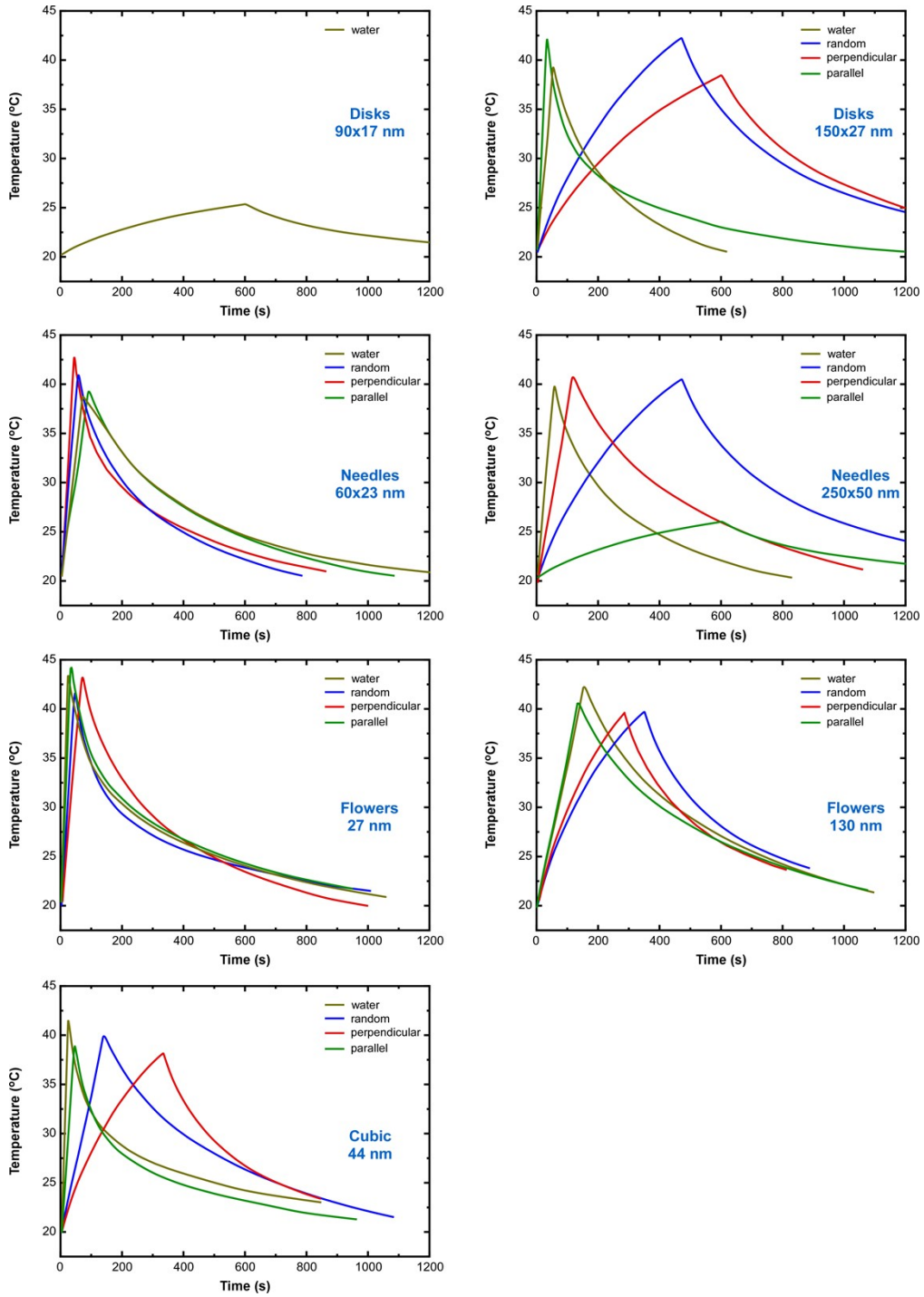

Fig. S6. Temperature versus time heating and cooling curves of the different anisometric MNPs (90x17 nm disks; 155x27 nm disks; 60x23 nm spindles; 250x50 nm spindles; 27 nm flowers; 130 nm flowers; 44 nm nanocubes) under various dispersion and orientation scenarios: water (light green line), random (blue

line), perpendicular (red line) and parallel (green line). The frequency of the AC field was 765 kHz, and its amplitude 24 kA/m.

Table S2. SAR determined for the different morphologies and sizes in water or agar and different assembly in the agar media (random, parallel and perpendicular).

Sample	SAR_{water} (W/g_{Fe})	$SAR_{agar,\ random}$ (W/g_{Fe})	$SAR_{agar,\ ||}$ (W/g_{Fe})	$SAR_{agar,\ \perp}$ (W/g_{Fe})
Disks 90x17 nm	22	-	-	-
Disks 155x27 nm	915	107	1400	77
Spindles 60x23 nm	787	830	723	1323
Spindles 250x50 nm	820	77	61	323
Flowers 27 nm	1246	1084	2092	1000
Flowers 130 nm	350	230	415	292
Cubes 22 nm	1085	-	-	-
Cubes 44 nm	1606	400	1123	246

Table S3. Calculation of the volume per particle of the different morphologies and sizes presented and the corresponding normalized SAR values in water or in agar (at random, parallel and perpendicular assembly configurations).

Sample	Volume (nm^3)	SAR_{water}/Volume ($W/g_{Fe}{\cdot}nm^3 \cdot 10^{-4}$)	$SAR_{agar,random}$/Volume ($W/g_{Fe}{\cdot}nm^3 \cdot 10^{-4}$)	$SAR_{agar,\ ||}$/Volume ($W/g_{Fe}{\cdot}nm^3 \cdot 10^{-4}$)	($W/g_{Fe}{\cdot}nm^3 \cdot 10^{-4}$)
Disks 90x17 nm	89438	2.4	-	-	-
Disks 155x27 nm	426780	21	2.5	32	1.8
Spindles 60x23 nm	15205	517	545	475	870
Spindles 250x50 nm	84823	96	9.0	7.2	38
Flowers 27 nm	11494	2091	1084	1820	870
Flowers 130 nm	1150350	3.0	2.0	4.0	2.5
Cubes 22 nm	10648	1018	-	-	-
Cubes 44 nm	85184	188	47	131	29

6. Scanning Electron Microscopy (SEM) analysis of the 44 nm cubes in agar at random

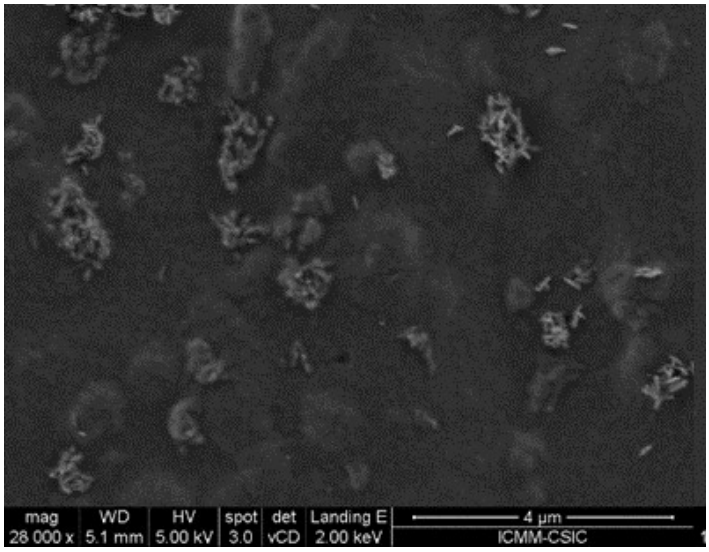

Fig. S7. SEM image of 250x50 nm spindles nanoparticles immobilized in agar viscous media at random configuration in the absence of the static magnetic field.

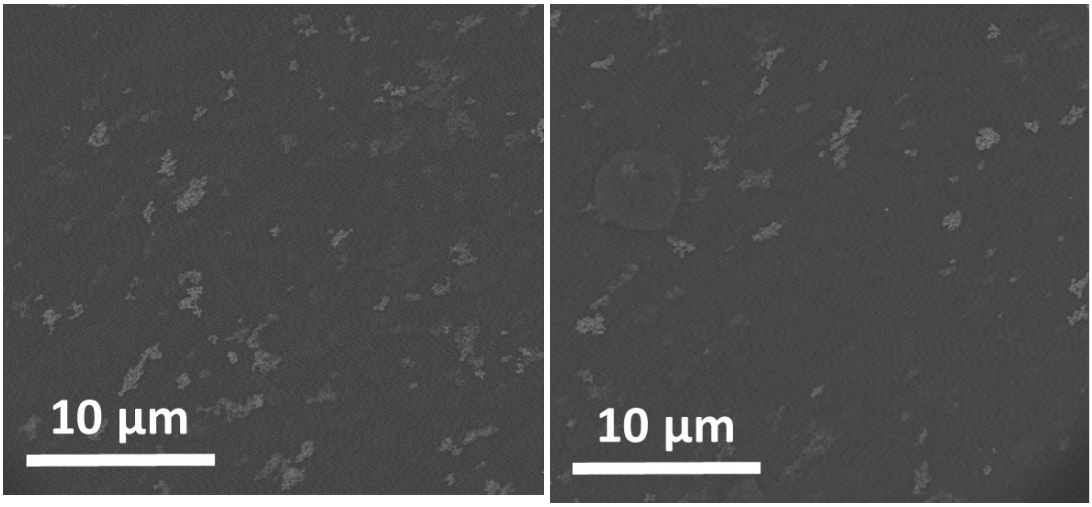

Fig. S8. SEM image of 44 nm cubic nanoparticles immobilized in agar viscous media at random configuration in the absence of the static magnetic field.

7. SEM analysis of oriented cubes, disks and flowers in viscous media in the presence of a magnet.

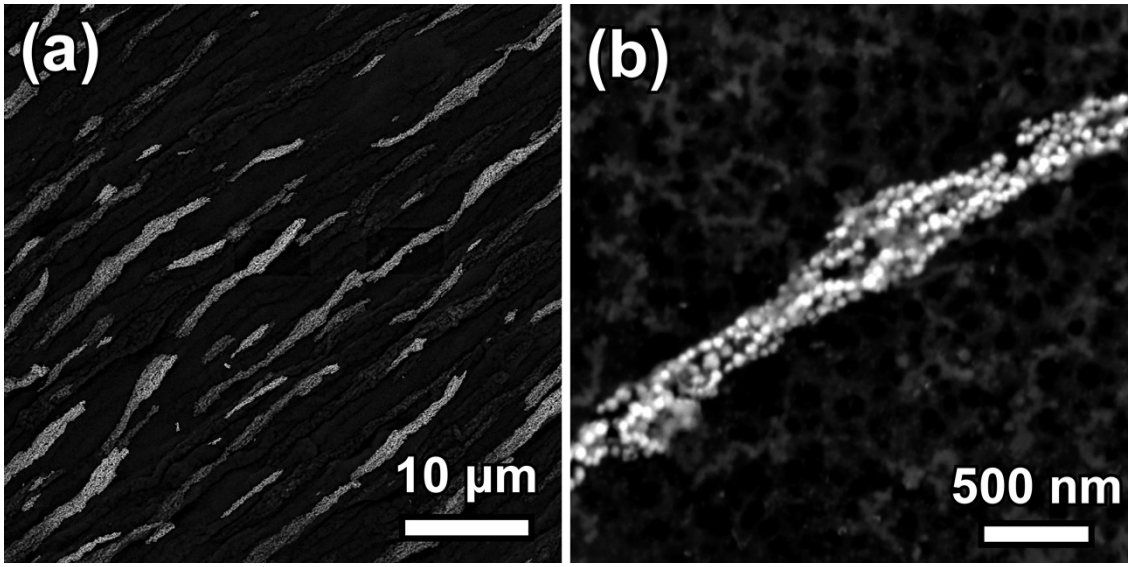

Fig. S9. Low (a) and high magnification (b) SEM images of successfully oriented 44 nm cubic nanoparticles.

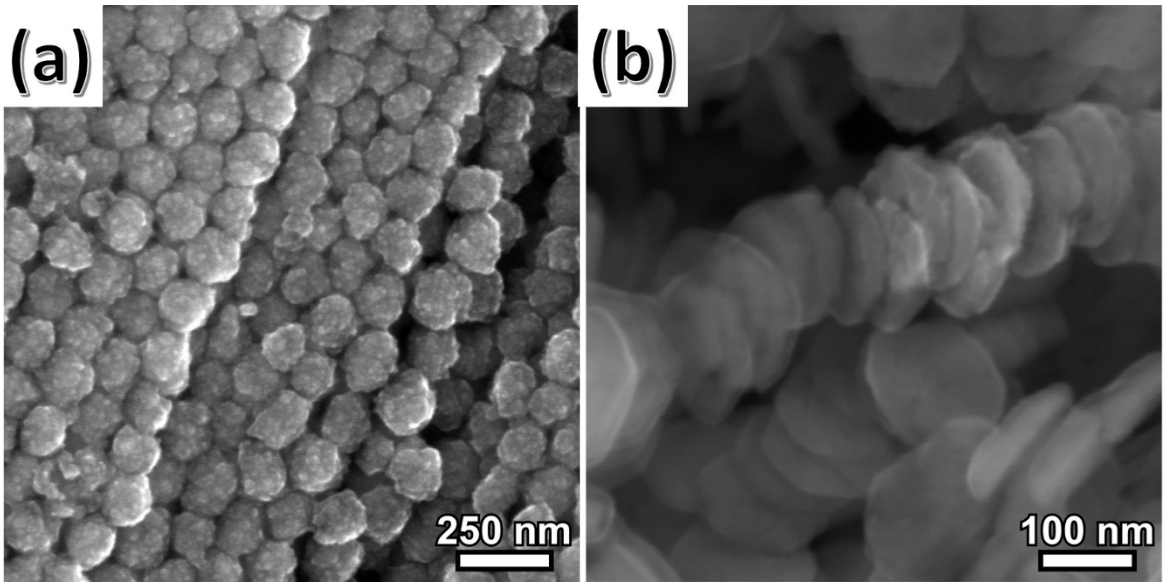

Figure S10. High magnification SEM images of successfully oriented nanoflowers (a) and nanodisks (b). While symmetrical MNPs like 130 nm nanoflowers promote highly ordered structures both at the micron- and nanoscale, MNPs with higher aspect ratio like 155x27 nm disks form ordered structures in the microscale, but in the nanoscale, they clearly form pillars interacting face to face., which are not perfectly straight but display certain displacement with each other.

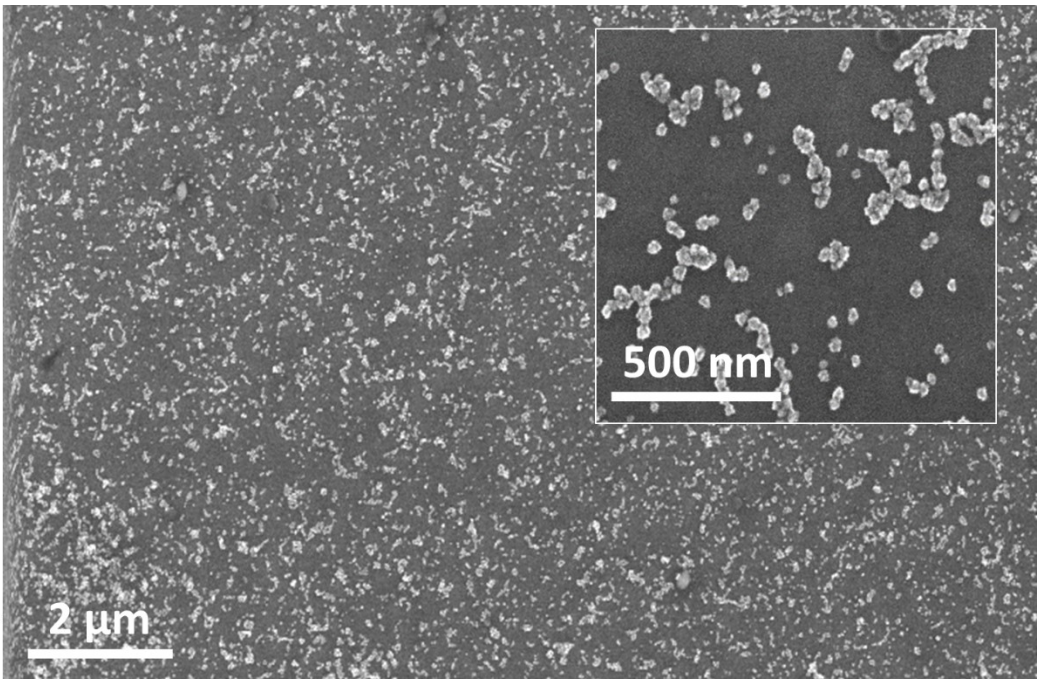

Fig. S11. SEM image showing the formation of nano-sized chains of 27 nm nanoflowers when this system of MNPs is immobilized in agar in the presence of a static magnetic field.

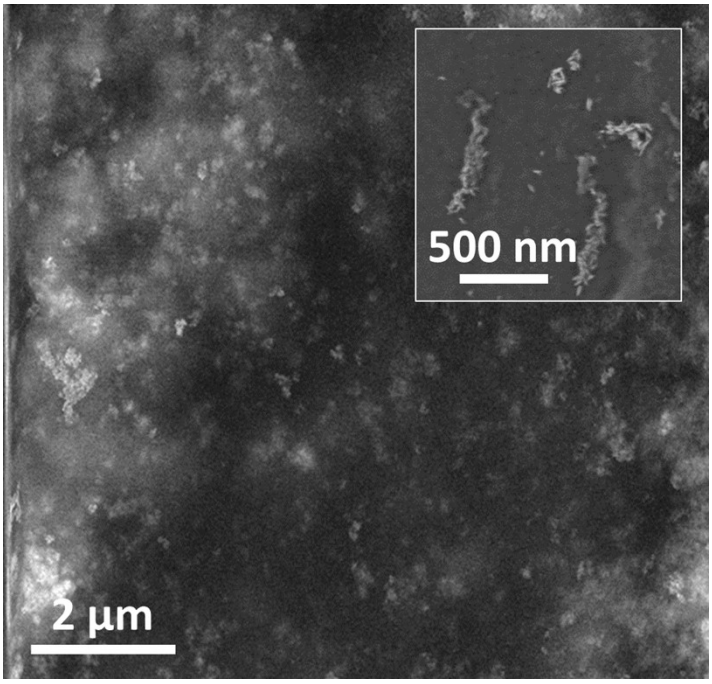

Fig. S12. SEM image showing the formation of nano-sized chains of 60x23 nm spindles when this system of MNPs is immobilized in agar in the presence of a static magnetic field. Inset: SEM image at higher magnification showing the formation of the nano-chains.

8. Minor loops recorded for the 44 nm nanocubes

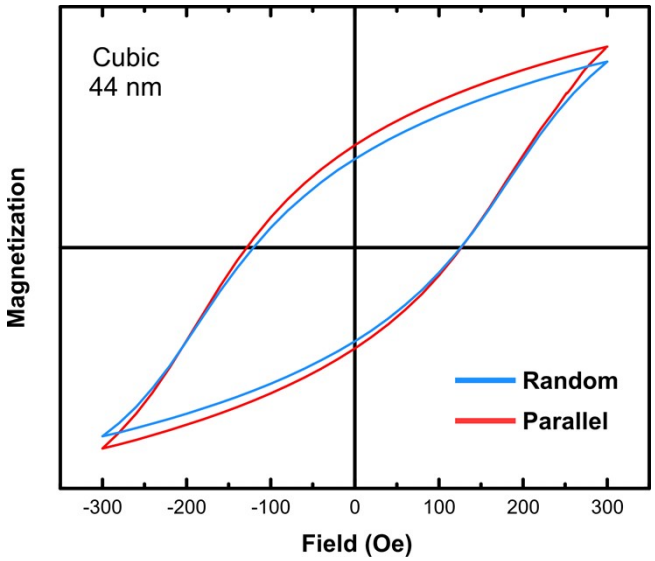

Figure S13. Minor loops at 300 Oe of oriented and random distributed 44 nm cubic nanoparticles in agarose gel.

9. General remarks, advantages and disadvantages of the presented theoretical approach:

Please note that there are other computational approaches that might offer advantages over the current one, based on the Landau-Lifshitz-Gilbert equation. The major advantage of the use of the LLG equation is that real-time dynamics and various anisotropy terms can be properly treated by the equation [1,2]. It is also appropriate for investigating non-coherent magnetization processes with sub-grain discretization. Furthermore, the LLG can be coupled with a rotation equation, thereby allowing the description of the particle properties in a viscous media, where its orientation with respect to the field direction may evolve over time [3,4]. However, it is highly demanding on computational resources. Alternatively, the standard Metropolis Monte Carlo (MMC) has been successfully applied to study interacting systems of magnetic nanoparticles [5,6], but has two main limitations: it is based on the dipole-dipole approximation (i.e., shape can only be treated indirectly, through the effective anisotropy [7]), and lacks real time dynamics. The real-time dynamics can be properly treated by means of the so-called kinetic Monte Carlo (kMC) [8,9,10]. Kinetic Monte Carlo is a statistical approach based on the Arrhenius-Neel law (high energy barriers) and thus requires knowledge of energy barriers and the prefactor. The energy barriers are calculated typically in some approximation (valid for very weakly interacting systems) and the prefactor is typically taken as a constant (while known to be dependent on many parameters). While methods exist to calculate energy barriers and prefactor more exactly, these simulations are feasible for small systems only [11]. Although the model is relatively straightforward for uniaxial anisotropy, the introduction of higher order anisotropies, for example cubic anisotropy [12] is non-trivial and has yet to be applied in the context of hyperthermia. Wherever feasible, the recommendation should be to use the LLG equation and revert to MC and kMC methods, especially for systems of large numbers of particles.

REFERENCES

1. M. S. Carrião et al., J. Appl. Phys. 121, 173901 (2017).

2. C. Haase and U. Nowak, Phys. Rev. B 85, 045435 (2012).

3. N. Usov and B. Y. Liubimov, J. Appl. Phys. 112, 023901 (2012).

4. H. Mamiya and B. Jeyadevan, Sci. Rep. 1, 1 (2011).

5. D. Serantes et al., J. Appl. Phys. 108, 173918 (2010).

6. I. Conde-Leboran et al., J. Phys. Chem. C 119, 15698 (2015).

7. C. Martinez-Boubeta et al., Sci. Rep. 3, 1652 (2013).

8. S. Ruta et al., Sci. Rep. 5, 9090 (2015).

9. D. Niculaes et al., ACS Nano 11, 12121 (2017).

10. M. Anand et al., Phys. Rev. B 99, 024402 (2019).

11. O. Chubykalo-Fesenko and R. W. Chantrell, IEEE Trans. Magn. 41, 3103 (2005).

12. M Walker et al., J. Phys.: Condens. Matt. 5, 2779 (1993).